EMBO reports

scientific report

Dynamic states of the DNA repair enzyme AlkB regulate product release

Boris Bleijlevens[1†], Tara Shivarattan[1], Emily Flashman[2], Yi Yang[1], Pete J. Simpson[1], Pertti Koivisto[3], Barbara Sedgwick[3], Christopher J. Schofield[2] & Steve J. Matthews[1+]

[1]Division of Molecular Biosciences, Faculty of Natural Sciences, Imperial College London, South Kensington Campus, London, UK, [2]The Chemistry Research Laboratory and OCISB, University of Oxford, Oxford, UK, and [3]Cancer Research UK London Research Institute, Clare Hall Laboratories, South Mimms, Hertfordshire, UK

The 2-oxoglutarate (2OG)- and Fe^{2+}-dependent dioxygenase AlkB couples the demethylation of modified DNA to the decarboxylation of 2OG. Extensive crystallographic analyses have shown no evidence of significant structural differences between complexes binding either 2OG or succinate. By using nuclear magnetic resonance spectroscopy, we have shown that the AlkB–succinate and AlkB–2OG complexes have significantly different dynamic properties in solution. 2OG makes the necessary contacts between the metal site and the large β-sheet to maintain a fully folded conformation. Oxidative decarboxylation of 2OG to succinate leads to weakening of a main contact with the large β-sheet, resulting in an enhanced dynamic state. These conformational fluctuations allow for the replacement of succinate in the central core of the protein and probably contribute to the effective release of unmethylated DNA. We also propose that the inherent dynamics of the co-product complex and the subsequent increased molecular ordering of the co-substrate complex have a role in DNA damage recognition.

Keywords: AlkB; DNA repair; protein folding; protein–nucleic acid interactions

EMBO reports (2008) **9**, 872–877. doi:10.1038/embor.2008.120

INTRODUCTION

Alkylating agents constitute a large class of DNA-damaging agents that generate both mutagenic and cytotoxic DNA lesions. Much of our understanding of alkylation damage repair is from studies on *Escherichia coli*, in particular on the adaptive (Ada) response, which involves the upregulation of four genes: *ada*, *aidB*, *alkA* and *alkB* (Sedgwick *et al*, 2007). The Ada protein is a multifunctional DNA methyltransferase that also acts as a transcriptional activator of the response. The exact function of AidB, a flavin-binding protein, remains to be explained and AlkA is a DNA glycosylase with a broad specificity. AlkB catalyses the demethylation of 1-methyladenine and 3-methylcytosine in DNA and RNA, coupled to the decarboxylation of 2-oxoglutarate (2OG) to succinate and CO_2 (Falnes *et al*, 2002; Trewick *et al*, 2002). Homologues of AlkB have been identified in species ranging from bacteria to humans; eight human homologues (ABH) have been described, but only two, ABH2 and ABH3, are known to repair DNA/RNA damage (Duncan *et al*, 2002; Aas *et al*, 2003).

The dioxygenase family to which AlkB belongs is ubiquitous and renowned for its catalytic versatility. Despite often low overall sequence similarity, these enzymes share an absolute requirement for Fe^{2+} and a near-absolute requirement for 2OG. They are characterized by a highly conserved metal-binding motif and 2OG co-substrate-binding motifs that are characteristic of different subfamilies. Crystallographic studies of the 2OG dioxygenases and related enzymes have shown a common double-stranded β-helix (DSBH) fold that acts as a platform for the presentation of conserved elements of the catalytic machinery. The structures mainly vary in the elements (including helices) that surround and support the core region and contribute to selectivity (Clifton *et al*, 2006).

Crystal structures of AlkB and its human homologue ABH3 have shown similar overall folds (Sundheim *et al*, 2006; Yu *et al*, 2006). The DSBH centre comprises a large β-sheet (formed by β-strands C1, C8, C3 and C6) and a smaller β-sheet (C2, C7, C4 and C5), which sandwich the metal- and cofactor-binding pocket (supplementary Fig S6 online). Two distinct regions in the DSBH can be differentiated: the highly conserved metal-binding region, which contains the $H_{131}xD_{133}x_nH_{187}$ Fe^{2+} coordinating triad presented by the minor β-sheet, and the major β-sheet, which contains the 2OG-binding $R_{204}xNxTxR_{210}$ motif (numbering of the residues as in the AlkB structure; Yu *et al*, 2006). The

[1]Division of Molecular Biosciences, Faculty of Natural Sciences, Imperial College London, South Kensington Campus, London SW7 2AZ, UK
[2]The Chemistry Research Laboratory and OCISB, University of Oxford, Oxford OX1 3TA, UK
[3]Cancer Research UK London Research Institute, Clare Hall Laboratories, South Mimms, Hertfordshire EN6 3LD, UK
[†]Present address: Department of Medical Biochemistry, Academic Medical Center, University of Amsterdam, Amsterdam, The Netherlands
[+]Corresponding author. Tel: +44 (0)207 594 5315; Fax: +44 (0)207 594 5207; E-mail: s.j.matthews@imperial.ac.uk

Received 26 September 2007; revised 19 May 2008; accepted 23 May 2008; published online 11 July 2008

1-carboxylate and 2-oxo groups of 2OG bind to the metal in a bidentate manner, whereas the 5-carboxylate of 2OG interacts by means of a hydrogen bond with Arg 210 and by means of a salt bridge with Arg 204 (Yu *et al*, 2006). The DSBH core is supported by two amino-terminal α-helices and a small β-sheet (L1, L2 and L3) that acts as a substrate-binding lid. AlkB interacts with DNA by means of many hydrogen bonds between the nucleotide backbone phosphates and Thr 51, Tyr 76 and Arg 161. The methylated base is flipped out relative to the flanking bases and stacked in a hydrophobic cavity between residues Try 69 and His 131 with its methyl group pointing towards the metal (Yu *et al*, 2006). Crystal structures have been reported for AlkB–metal complexes in the presence of 2OG and succinate, both with DNA. The ABH3 X-ray structure was solved in complex with 2OG but without DNA. None of the crystallographic studies on AlkB, nor those on any other member of the 2OG-dependent non-haem Fe^{2+} dioxygenase family, has shown significant changes in the overall protein fold induced by the presence or absence of metal, 2OG or succinate (Clifton *et al*, 2006). The crystallographic data do not explain how AlkB discriminates between 2OG and succinate, neither do they show details about uptake and release of substrate and product, respectively. The nature of 2OG/succinate binding to 2OG oxygenases is also of interest, as abnormally high levels of the tricarboxylic acid cycle intermediates fumarate and succinate have been proposed to modulate the activity of 2OG oxygenases, including the prolyl hydroxylase domain enzymes, involved in the hypoxic response through competition for binding with 2OG (Selak *et al*, 2005; Hewitson *et al*, 2007); this competition is proposed as a molecular explanation for the Warburg effect in cancer cells.

To answer the question of how binding of 2OG and succinate is related to substrate specificity, we used an integrated approach involving structural and biophysical techniques. Here, we present evidence that AlkB undergoes a major transition in dynamics between the 2OG and the succinate complexes, and propose that this transition is important for the release of products from AlkB. Moreover, this dynamic behaviour might represent a general mechanism for regulating product release by 2OG oxygenases.

RESULTS

Circular dichroism spectroscopy

The effects of co-substrate (2OG) and co-product (succinate) binding on the secondary structure were investigated by using far-ultraviolet circular dichroism (CD) spectroscopy (Fig 1). In this region, AlkB complexes show a negative band at 214 nm and a maximum at 195 nm. Spectral fitting indicates mainly β-sheet structure (39%) with a much smaller (<10%) helical contribution, which is in agreement with the X-ray structure (Yu *et al*, 2006). The secondary structure content does not change significantly when either 2OG or succinate is bound.

Nuclear magnetic resonance spectroscopy

The one-dimensional (1D) ^{1}H nuclear magnetic resonance (NMR) spectrum of the AlkB–Fe^{2+}–succinate complex shows several resonances in the up-field methyl region (between 0.5 and −1.5 ppm; Fig 2). However, the AlkB–Fe^{2+}–2OG complex shows significantly more resonances in this region. Increased dispersion and sharpening of these signals are consistent with a structural transition and the formation of a globular, rigidly tumbling domain. AlkB–Co^{2+} complexes also show more resonances in the up-field methyl region with 2OG than with succinate (Fig 2).

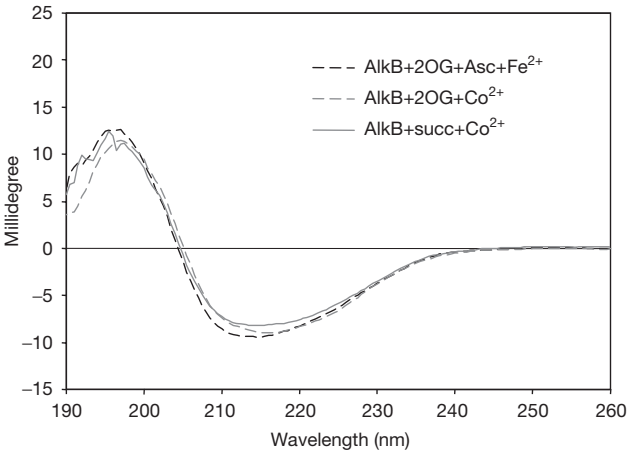

Fig 1 | Binding of metal (Fe^{2+} or Co^{2+}) and cofactor (2OG/succinate) to AlkB monitored by using far-ultraviolet circular dichroism spectroscopy. Ascorbate (1 mM) was added to keep Fe^{2+} in a reduced state. 2OG, 2-oxoglutarate; Asc, ascorbate; succ, succinate.

The two-dimensional ^{15}N-^{1}H heteronuclear single quantum coherence (HSQC) spectrum of the AlkB–Fe^{2+}–2OG complex is well dispersed (Fig 2) and was suitable for backbone assignment, as described previously (Shivarattan *et al*, 2005). Sixteen non-proline residues were not observed (total sequence 216 amino acids, 18 proline residues); most of these mapped to regions close to the metal centre coordinated to the protein by His 131, Asp 133 and His 187. The non-haem Fe^{2+} in 2OG-dependent dioxygenases can be bound in a paramagnetic high-spin ($S=2$) state (Solomon *et al*, 2003). Increased spectral width allowed the observation of resonances experiencing pseudo-contact shifts in the ^{1}H NMR spectrum, confirming the presence of a paramagnetic centre. The spin–spin relaxation rate of nuclei proximal to a paramagnetic centre is enhanced owing to contributions from dipolar interactions with unpaired electrons, resulting in significantly broader and often absent resonances (Bertini *et al*, 2004). Several broadened resonances fall outside the range influenced by the paramagnetic centre; most of these localize to the mobile substrate-binding lid and are most probably affected by conformational exchange.

The two-dimensional ^{15}N-^{1}H HSQC spectrum of the AlkB–Fe^{2+}–succinate complex is different from that of the 2OG complex (Fig 2). Most notable is the decrease in the intensity of 13 peaks in the spectrum of the succinate complex. In the AlkB–Fe^{2+}–2OG complex, these peaks are assigned to residues Met 49, Ala 60, Thr 71, Asn 120, Arg 121, Val 146, Leu 148, Phe 154, Gly 157, Leu 184, Asn 206, Gln 211 and Ala 212. In the succinate–Fe^{2+} complex, these resonances are severely broadened, mainly beyond detection. This is most probably due to local conformational exchange, which is indicative of an increase in molecular dynamics. A further 25 peaks show significant chemical shift changes between the 2OG and the succinate complex, indicating changes in chemical environment (see the supplementary information online for a complete list). Mapping of

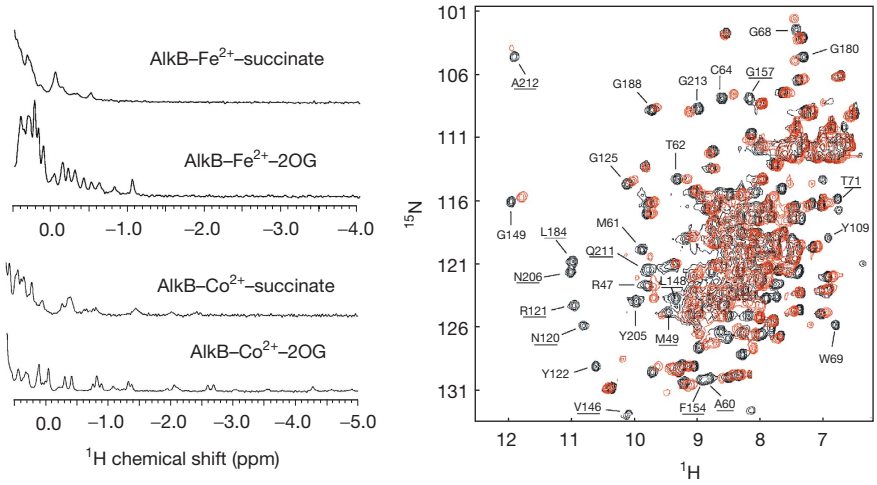

Fig 2 | Nuclear magnetic resonance spectroscopic analysis of complexes of AlkB. Left: methyl regions of one-dimensional ^{1}H nuclear magnetic resonance (NMR) spectra of Fe^{2+} and Co^{2+} complexes of AlkB. Right: overlay of the two-dimensional ^{15}N-^{1}H heteronuclear single quantum coherence (HSQC) NMR spectra of the AlkB–Fe^{2+}–2OG (black) and the AlkB–Fe^{2+}–succinate complex (red). Spectra were recorded at 303 K. Severely broadened residues are underlined. Only part of the shifting residues are labelled owing to space constraints; a complete list of shifting residues is presented in the supplementary information online. 2OG, 2-oxoglutarate.

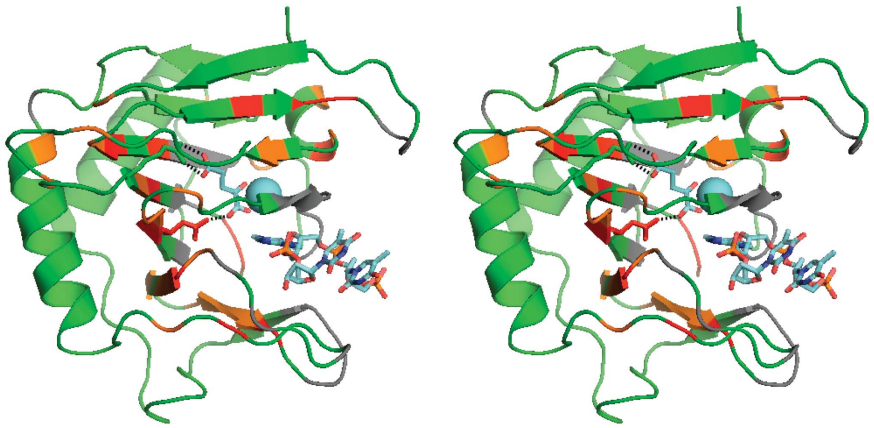

Fig 3 | Stereo view of the structural changes in AlkB. Mapping of residues sensitive to the 2OG–succinate transition on the structure of AlkB. Shifting residues are shown in orange and disappearing residues in red, illustrating 'hot', flexible areas in the succinate complex. Residues in grey were not detected in the nuclear magnetic resonance experiments. The Fe^{2+} ion is shown as a blue sphere, and 2OG and DNA are shown as sticks. The side chain of residue Asn 120 interacting with 2OG is also shown as sticks. 2OG, 2-oxoglutarate.

disappearing (red) and shifting residues (orange) on the crystal structure of the 2OG complex (Fig 3) shows that the affected residues are predominantly located in strands C1 and C8 of the large β-sheet, close to where 2OG makes contact with Asn 120. Interestingly, the *B*-factors of the various AlkB complexes do not indicate increased protein mobility in this region (supplementary Fig S6 online). The NMR data also indicate increased dynamics in other parts of the protein, most notably strands L1 and L2 that form the DNA-binding lid. The two-dimensional NMR characteristics of AlkB reconstituted with Co^{2+} are consistent with those observed for the analogous iron complexes (supplementary Fig S7 online). Equilibrium fluorescence experiments further support this idea of increased dynamics in the AlkB–succinate complex (supplementary information and supplementary Fig S8 online). Clear differences are observed in the acrylamide fluorescence quenching characteristics between the succinate and the 2OG complex. All four tryptophan residues in the AlkB–Co^{2+}–succinate complex are accessible to solvent, characteristic of a relatively open and flexible complex. By contrast, tryptophan fluorescence in the AlkB–Co^{2+}–2OG complex is quenched less easily, which is indicative of a more rigid complex.

DNA binding

In light of the differences in protein dynamics, binding of single-stranded DNA to the AlkB–Fe^{2+}–2OG and the AlkB–Fe^{2+}–succinate complexes was studied by using isothermal

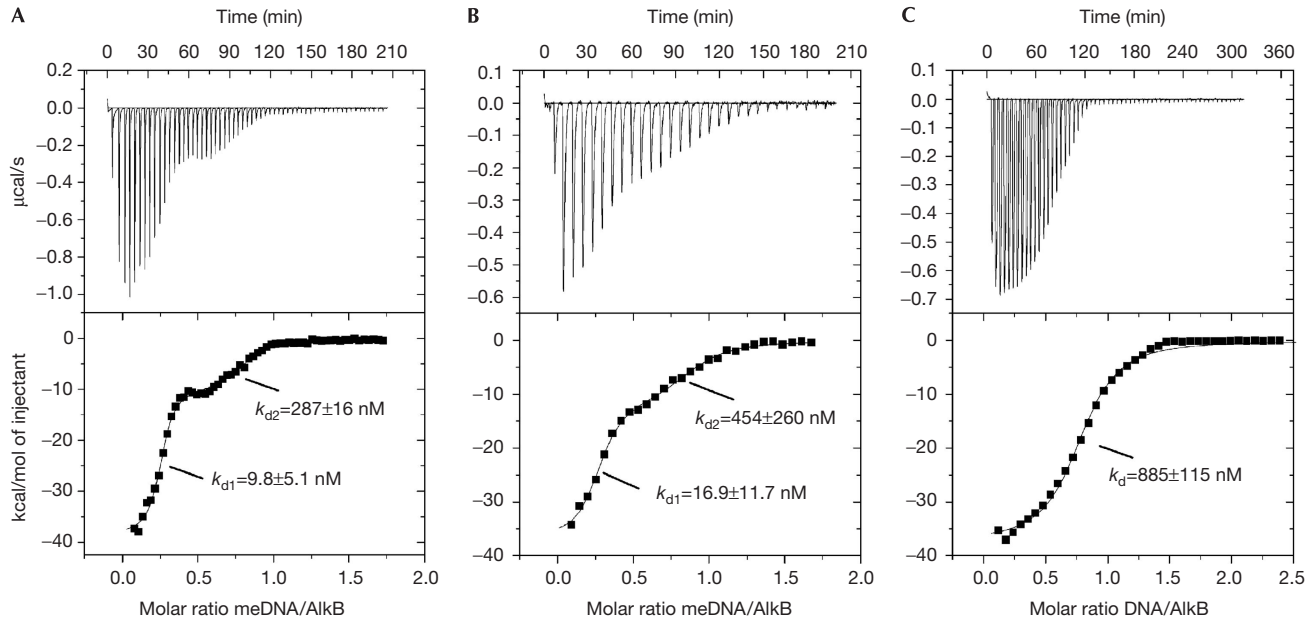

Fig 4 | Isothermal calorimetric titrations of DNA binding to various complexes of AlkB. (**A**) The initial enzyme–substrate complex: T-1meA-T to AlkB–Fe^{2+}–2OG. (**B**) T-1meA-T to AlkB–Fe^{2+}–succinate. (**C**) The complex at the end of the catalytic cycle: unmethylated DNA (TTCTT) to AlkB–Fe^{2+}–succinate. Top: Calorimetric titration profile of aliquots of DNA into AlkB. Bottom: Least squares fit of heat absorbed per mole of titrant versus DNA/AlkB ratio. Binding curves were fitted as two independent binding events for (**A**,**B**) and a single binding event for (**C**). Constants are averages of two measurements. meDNA, methylated DNA; 2OG, 2-oxoglutarate.

titration calorimetry (ITC; Fig 4). Binding affinities of several complexes were compared: (i) methylated DNA (meDNA) bound to AlkB–Fe^{2+}–2OG, as this is the starting point of catalysis; (ii) meDNA bound to AlkB–Fe^{2+}–succinate to assess the effect of increased protein dynamics; and (iii) unmethylated DNA bound to AlkB–Fe^{2+}–succinate, as this represents the final state complex after catalysis. We consistently observed biphasic binding isotherms for binding of meDNA to various AlkB complexes. As the ^{1}H NMR spectrum of meDNA showed no evidence of sample heterogeneity (data not shown), the biphasic binding curve is attributed to the presence of two AlkB species with different binding affinities for meDNA. The presence of the lower-affinity form is most probably due to the oxidative self-inactivation of AlkB, in which the proximal side chain of Try 178 is hydroxylated, resulting in subtle alterations near the active site, which is a commonly observed characteristic for this class of enzymes (Henshaw *et al*, 2004). Furthermore, oxidation of Leu 177 in ABH3 (Leu 118 in AlkB) has been proposed to interfere with meDNA binding. Oxidation of this residue was observed in anaerobically prepared samples of both ABH3 and AlkB, indicating that this modification is generated during protein expression (Sundheim *et al*, 2006). The idea that this modification might sterically interfere with binding of the methyl group of meDNA is supported by the current observations. However, at this stage, we cannot exclude the possibility of oxidation of the Fe^{2+} site in the course of the ITC experiment, possibly changing the affinity of the complex for DNA. Oxidative modifications did not seem to affect binding of unmethylated DNA, as the observed binding isotherms could be fitted to a one-binding-site model.

Binding of meDNA to the high-affinity AlkB–2OG complex is tight ($k_{d1} = 9.8 \pm 5.1$ nM), as might be expected for an enzyme–substrate complex. The lower-affinity species binds to meDNA considerably more weakly ($k_{d2} = 287 \pm 16$ nM). Binding of meDNA to the AlkB–succinate complex ($k_{d1} = 16.9 \pm 11.7$ nM, $k_{d2} = 454 \pm 260$ nM) is moderately weaker, suggesting that the increase in protein flexibility contributes to a reduced affinity for DNA. In the final state complex, the affinity of the AlkB–succinate complex for unmethylated DNA is significantly lower ($k_{d} = 885 \pm 115$ nM). Our data show that binding of DNA is an enthalpically driven process that counteracts the large entropic contributions resulting from a higher degree of ordering in the DNA-bound complex (supplementary information online; supplementary Table 1 online). In the absence of DNA, our NMR data and the *B*-factors observed in the X-ray structure show that the substrate-binding lid is dynamic (supplementary Fig S6 online; Yu *et al*, 2006). We propose that on binding of DNA, this region becomes (more) structured, resulting in a decrease in entropy, which is compensated for by a large favourable enthalpic contribution. An earlier study reported a much lower affinity ($k_{d} \sim 40\,\mu$M) for the interaction of AlkB with DNA than that reported here (Mishina *et al*, 2004). We estimate that only a fraction of the protein in these experiments, which was purified endogenously from *E. coli*, contained both Fe^{2+} and 2OG, as we have measured similar binding curves for DNA binding to AlkB samples that were made completely devoid of metal (supplementary Fig S9 online). Binding of T-1meA-T to an inhibited AlkB–Fe complex induced clear chemical shift changes (supplementary Fig S10 online). Titration of meDNA to AlkB showed that these interactions are in a slow-exchange regime, which is

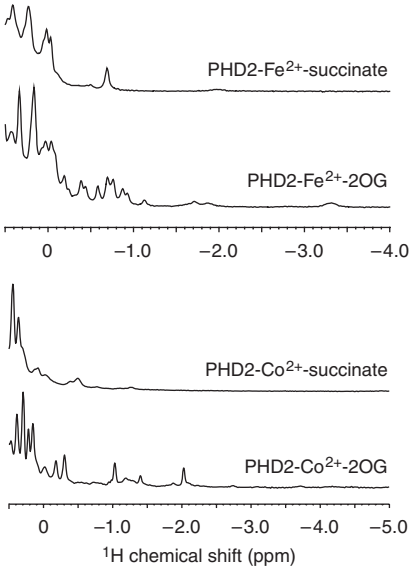

Fig 5 | Methyl region of one-dimensional ^{1}H nuclear magnetic resonance spectra of PHD2 complexes, at 298 K. 2OG, 2-oxoglutarate; PHD2, prolyl hydroxylase domain-containing protein 2.

indicative of tight binding. From these data, an upper limit of 500 nM for the k_d could be estimated, independently confirming the tight binding observed in the ITC experiments (supplementary information online).

Interestingly, the dynamic behaviour that we consistently observe for AlkB has not been reported previously for any of the related 2OG-dependent dioxygenases. Although conformational changes have been observed on substrate binding, X-ray crystal structures of the apo and holo forms of related enzymes show negligible structural differences (Clifton *et al*, 2006), suggesting that this characteristic is perhaps generalized among 2OG-dependent dioxygenases that process large oligomeric substrates, such as AlkB. To investigate this issue, we examined another member of the 2OG-dependent, non-haem iron dioxygenases that acts on a large substrate: prolyl hydroxylase domain-containing protein 2 (PHD2), for which crystallographic data are available (McDonough *et al*, 2006). The physiological substrate of PHD2 is the α-subunit of hypoxia-inducing transcription factor (HIF-α), a 92.6 kDa protein. The levels of HIF-α are regulated by PHD2 through the post-translational hydroxylation of either of two prolyl residues, which provide a signal for HIF-α degradation by the ubiquitin–proteasome system. PHD2 forms an unusually stable enzyme–Fe^{2+}–2OG complex, even under aerobic conditions (binding constants for Fe^{2+} and 2OG are $\ll 1$ and $< 2\,\mu M$, respectively; McNeill *et al*, 2005). AlkB has also been reported to co-purify with 2OG (Mishina *et al*, 2004), suggesting that both AlkB and PHD2 share a common property of binding tightly to 2OG. Interestingly, the one-dimensional ^{1}H NMR spectra of PHD2 indicate that PHD2 shows changes in dynamics, similar to AlkB (Fig 5). When in a complex with succinate and Fe^{2+}, PHD2 shows a limited number of up-field resonances together with other broad signals associated with protons in the immediate vicinity of the paramagnetic Fe^{2+} ion. The NMR spectrum of the 2OG-bound complex of PHD2 clearly shows an increasing number of up-field resonances indicative of a well-folded complex. In line with our observations with AlkB, complexes of PHD2 with Co^{2+} showed a similar behaviour (Fig 5). These initial results on PHD2, a system closely related to AlkB, show that this distinctive dynamic behaviour is not restricted to AlkB.

DISCUSSION

From the X-ray data, we conclude that an important site of interaction of 2OG with AlkB is the side chain of Asn 120, which is in close enough in proximity to form a hydrogen bond with the 1-carboxylate site of 2OG, but not with succinate (supplementary Fig S11 online). It is exactly this functional group that is released as carbon dioxide in the oxidative decarboxylation of 2OG to succinate. This results in the loss of contact between the organic co-substrate and Asn 120, breaking one of the connections between the two sheets of the DSBH. In addition, the resonance associated with Asn 120 in the HSQC NMR spectrum of the 2OG complex is broadened beyond detection in the spectrum of the succinate complex. Resonances assigned to neighbouring residues in the large β-sheet of the DSBH and the adjacent DNA-binding lid are also affected (Fig 3). Indeed, mutation of Asn 120 to Ala renders the 2OG complex more dynamic, resulting in similar NMR spectral properties for both succinate and 2OG complexes (supplementary Fig S12 online). In the N120A mutant, 2OG is no longer able to make the necessary contacts with the large β-sheet to maintain the active site geometry, contributing to a more dynamic 2OG complex. In this context, it is worth noting that the residue Asn 120 is conserved in six of the eight human ABH homologues of AlkB, most importantly in both ABH2 and ABH3, both of which are known to act on DNA/RNA. Mutation of the analogous residue in ABH3 decreases its activity by 60% (Sundheim *et al*, 2006). In PHD2, Tyr 303 is in a position to form a hydrogen bond with the 1-carboxylate of 2OG and to perform a similar role (supplementary Fig S11 online).

AlkB crystal structures show that the co-substrate and co-product are deeply buried within the protein and no channels exist for the efficient replacement of succinate by 2OG. A transition to an open and dynamic state with increased accessibility to the active site provides a plausible mechanism for the release of succinate and replenishment of 2OG at the end of the catalytic cycle. Preliminary ITC data show that succinate is also efficiently replaced by 2OG when the AlkB–Fe^{2+}–succinate complex binds to DNA (data not shown). We also propose that the dynamic behaviour of the AlkB–succinate complex contributes to lowering the efficiency for DNA binding. The AlkB–2OG complex has a stable, preformed, DNA-binding groove together with a primed substrate-binding lid that provides all the necessary contacts for optimal substrate binding. Consequently, to reduce the affinity for DNA, substantial changes in the protein's configuration are required to weaken the nonspecific DNA–protein interactions and efficiently release the DNA product. The lowered affinity for product DNA and the dynamic state of the AlkB–succinate complex favour a more transient interaction with DNA that would promote one-dimensional scanning for further nucleotide damage. The inherent dynamics of the succinate complex assists in the replenishment of the catalytic active site with 2OG, whereas increased affinity for meDNA confirms damage and allows subsequent repair by the 2OG complex. The results for PHD2, which parallel those for AlkB, suggest that the formation of

dynamic catalytic intermediates also applies to other members of the 2OG dioxygenase family, more particularly those acting on large oligomeric substrates.

METHODS

Protein expression and purification. Recombinant, full-length, carboxy-terminally His_6-tagged *E. coli* AlkB was expressed as a soluble protein in *E. coli* BL21 (DE3) bearing a recombinant plasmid derived from pET21b (Shivarattan *et al*, 2005). ^{15}N-labelled protein was produced in M9 minimal media containing $^{15}NH_4Cl$. N-terminally truncated human $PHD2_{181-426}$ was produced and purified, as described previously (McNeill *et al*, 2005). Protein concentrations were measured by the Bradford method or the A_{280} method ($\varepsilon_{280} = 31\ mM^{-1}\ cm^{-1}$). Details are provided in the supplementary information online. AlkB–Fe^{2+} complexes are unstable under aerobic conditions owing to the damaging effect of self-oxidation in the presence of both O_2 and 2OG (Henshaw *et al*, 2004); therefore, we investigated the possibility of metal replacement. The AlkB–Co^{2+} complex was shown to be stable under aerobic conditions; activity measurements showed that this complex was unable to activate O_2 and catalyse the demethylation of meDNA (data not shown). The crystal structures of the Co^{2+} and the Fe^{2+} complexes are nearly identical (Yu *et al*, 2006). In view of its increased stability under aerobic conditions and structural similarity to the native complex, the AlkB–Co^{2+} complex was used for the fluorescence and CD studies.

CD spectroscopy. Spectra were recorded on a Chirascan CD spectrometer (Applied Photophysics, Leatherhead, UK). Far-ultraviolet (190–260 nm) spectra were recorded in a 1-mm path length quartz cuvette at 20 °C. Concentrations were 12.5 μM (0.3 mg/ml) AlkB in 1 mM Tris–HCl, pH 7.6. Spectra were corrected for background signals from buffer and/or cofactors.

NMR spectroscopy. NMR data were recorded as described previously (Shivarattan *et al*, 2005). Three-dimensional ^{1}H-^{15}N/^{13}C nuclear Overhauser enhancement spectroscopy (NOESY)-HSQC (mixing time 100 ms at 500 MHz) experiments provided the inter-proton distances. ^{1}H-^{15}N NOESY data of the AlkB–Fe^{2+}–2OG complex were recorded. Unambiguous long-range nuclear Overhauser effects (NOEs) were used to reinforce the topology of the AlkB–Fe^{2+}–2OG complex in solution. None of the measured NOEs violated the distance constraints imposed by the crystal structure. NMR samples contained 100 μM AlkB in 20 mM Tris–HCl, pH 7.6, 1 mM 2OG/succinate, 100 μM Fe^{2+} and 1 mM ascorbate.

Isothermal titration calorimetry. ITC experiments were performed on a MicroCal VP-ITC microcalorimeter at 25 °C. Data were fitted using the Origin software. Each titration consisted of 5 or 10 μl injections of DNA (200 μM) into a 1.4 ml sample cell containing 20 μM AlkB in 20 mM Tris–HCl (pH 7.6). To remove oxygen, ITC experiments were conducted in a background of dithiothreitol (2 mM) and ascorbate (2 mM). Before reconstitution of apoAlkB with Fe, solutions were thoroughly degassed.

Supplementary information is available at *EMBO reports* online (http://www.emboreports.org)

ACKNOWLEDGEMENTS

This research was supported by Cancer Research UK grant C16554 and the BBSRC. Acquisition of the Chirascan CD spectrometer was supported by BBSRC grant BB/C510859/1.

CONFLICT OF INTEREST

The authors declare that they have no conflict of interest.

REFERENCES

Aas PA *et al* (2003) Human and bacterial oxidative demethylases repair alkylation damage in both RNA and DNA. *Nature* **421:** 859–863

Bertini I, Fragai M, Lee YM, Luchinat C, Terni B (2004) Paramagnetic metal ions in ligand screening: the Co-II matrix metalloproteinase 12. *Angew Chem Int Ed* **43:** 2254–2256

Clifton IJ, McDonough MA, Ehrismann D, Kershaw NJ, Granatino N, Schofield CJ (2006) Structural studies on 2-oxoglutarate oxygenases and related double-stranded β-helix fold proteins. *J Inorg Biochem* **100:** 644–669

Duncan T, Trewick SC, Koivisto P, Bates PA, Lindahl T, Sedgwick B (2002) Reversal of DNA alkylation damage by two human dioxygenases. *Proc Natl Acad Sci USA* **99:** 16660–16665

Falnes PO, Johansen RF, Seeberg E (2002) AlkB-mediated oxidative demethylation reverses DNA damage in *Escherichia coli*. *Nature* **419:** 178–182

Henshaw TF, Feig M, Hausinger RP (2004) Aberrant activity of the DNA repair enzyme AlkB. *J Inorg Biochem* **98:** 856–861

Hewitson KS, Lienard BM, McDonough MA, Clifton IJ, Butler D, Soares AS, Oldham NJ, McNeill LA, Schofield CJ (2007) Structural and mechanistic studies on the inhibition of the hypoxia-inducible transcription factor hydroxylases by tricarboxylic acid cycle intermediates. *J Biol Chem* **282:** 3293–3301

McDonough MA *et al* (2006) Cellular oxygen sensing: crystal structure of hypoxia-inducible factor prolyl hydroxylase (PHD2). *Proc Natl Acad Sci USA* **103:** 9814–9819

McNeill LA, Flashman E, Buck MR, Hewitson KS, Clifton IJ, Jeschke G, Claridge TD, Ehrismann D, Oldham NJ, Schofield CJ (2005) Hypoxia-inducible factor prolyl hydroxylase 2 has a high affinity for ferrous iron and 2-oxoglutarate. *Mol Biosyst* **1:** 321–324

Mishina Y, Chen LX, He C (2004) Preparation and characterization of the native iron(II)-containing DNA repair AlkB protein directly from *Escherichia coli*. *J Am Chem Soc* **126:** 16930–16936

Sedgwick B, Bates PA, Paik J, Jacobs SC, Lindahl T (2007) Repair of alkylated DNA: recent advances. *DNA Repair* **6:** 429–442

Selak MA, Armour SM, MacKenzie ED, Boulahbel H, Watson DG, Mansfield KD, Pan Y, Simon MC, Thompson CB, Gottlieb E (2005) Succinate links TCA cycle dysfunction to oncogenesis by inhibiting HIF-α prolyl hydroxylase. *Cancer Cell* **7:** 77–85

Shivarattan T, Chen HA, Simpson P, Sedgwick B, Matthews S (2005) Resonance assignments of *Escherichia coli* AlkB: a key 2-oxoglutarate and Fe(II) dependent dioxygenase of the adaptive DNA-repair response. *J Biomol NMR* **33:** 138

Solomon EI, Decker A, Lehnert N (2003) Non-heme iron enzymes: contrasts to heme catalysis. *Proc Natl Acad Sci USA* **100:** 3589–3594

Sundheim O, Vagbo CB, Bjoras M, Sousa MML, Talstad V, Aas PA, Drablos F, Krokan HE, Tainer JA, Slupphaug G (2006) Human ABH3 structure and key residues for oxidative demethylation to reverse DNA/RNA damage. *EMBO J* **25:** 3389–3397

Trewick SC, Henshaw TF, Hausinger RP, Lindahl T, Sedgwick B (2002) Oxidative demethylation by *Escherichia coli* AlkB directly reverts DNA base damage. *Nature* **419:** 174–178

Yu B, Edstrom WC, Benach J, Hamuro Y, Weber PC, Gibney BR, Hunt JF (2006) Crystal structures of catalytic complexes of the oxidative DNA/RNA repair enzyme AlkB. *Nature* **439:** 879–884